Integration
geoscience
engineering
partnership
geoConvention 2013

Physical seismic modeling of a near-vertical fault zone

Jessie M. Arthur*, University of Calgary, CREWES, Calgary, Alberta
jmarthur@ucalgary.ca
and
Donald C. Lawton, University of Calgary, CREWES, Calgary, Alberta
and
Joe Wong, University of Calgary, CREWES, Calgary, Alberta

Summary

Detecting faults and subsequent deformation zones is significant in geotechnical engineering applications, seismic hazard assessment in earthquake studies, and the petroleum industry for reservoir potential where faults act as a conduit to migrate or trap hydrocarbon flow. Fault identification is also important in shale gas development to design better productive reservoir stimulation by accounting for the slow slip of pre-existing faults during hydraulic fracturing.

This study shows seismic physical modeling results for a shallow vertical fault zone with slight vertical throw. Several physical model prototypes were created with materials which range in velocity and density to best simulate host rock and a deformed fault zone. 2D marine seismic data were acquired and processed at the University of Calgary Seismic Physical Modeling Facility. Physical model materials tested include plaster, sandstone, limestone, lard, wax, and liquid acrylic.

The post-stack imaged results are compared and it can be seen that the fault zone is resolved in both zero offset and common source data from physical modeling. An interesting by-product from the physical modeling acquisition was the identification of ghost reflections captured later than the primary reflections, which could be used in ‘mirror imaging’, thus providing better illumination of the fault zone. The modeled fault zone images show close similarity to images from real 2D seismic data collected over a recent fault rupture in New Zealand.

Introduction

Detecting shallow fault zones is significant in geotechnical engineering applications and seismic hazard assessment in earthquake studies. The Greendale Fault in the Canterbury region of New Zealand was previously undetected when it ruptured to the ground surface during the Mw 7.1 Darfield earthquake in September, 2010. Shallow fault zones can be identified by high resolution seismic reflection profiling (Kaiser et al., 2011), as the deformation of rocks near the fault zone causes changes in lithology, pore pressure, and seismic velocity (Mooney and Ginzburg, 1986).

Fault identification is also important to the petroleum industry, where faults may either migrate or trap hydrocarbon flow. However, the effect of faults on a reservoir are complex and difficult to classify as each geologic environment is unique in terms of geometry, distribution, connectivity, and hydraulic properties (Aydin, 2000). A hydrocarbon trap can result from a sealed fault. Reservoirs in direct contact with sheared zones are sealed as a result of accumulated sheared sediment along the fault surface, whereas reservoirs bordering the fault surface are poorly sealed or not sealed (Berg and Avery, 1995). Active faults may act as a conduit to hydrocarbon flow along the fault plane, within the fault zone, and near the tips of active fault zones (Tamagawa and Pollard, 2008).

The identification of fault type is also important in reservoir potential. Improved reservoir performance is seen in areas that have a critically stressed strike-slip fault regime, where high ratios of shear to normal stress produce permeable fracture damage zones along the fault. This compares to lower reservoir potential in thrust fault stress regimes where fewer fractures with high shear stress ratios exist (Hennings et al., 2012).

Recognition of pre-existing faults is important in shale gas production using hydraulic fracturing to stimulate the reservoir rock. The physical and deformation mechanisms responsible for reservoir stimulation by hydraulic fracturing are complex and not yet fully understood (Zoback et al., 2012). Microseismic events are an indication of shear slip on faults and fractures caused by hydraulic fracturing used to increase production in unconventional resources. However, production of natural gas generated from hydraulic fracturing does not simply correlate with the number of microseismic events (Vermylen and Zoback, 2011). Recent studies have shown evidence of slow slip, which is indicated by long period, and long duration seismic events on pre-existing fault planes during stimulation, is shown to be a major contributing shear deformation mechanism that creates multiple permeable planes surrounding induced fractures (Das and Zoback, 2011). The need for better fault knowledge and subsequent deformation zone research is abundant. This study approaches fault detectability by seismic physical modeling, and compares the results to field data acquired across the surface ruptured Greendale Fault in New Zealand.

Seismic physical modeling provides scaled simulations of real-world scenarios with the benefit of controlled acquisition geometry and physical model properties (Lawton et al., 1998). Modeling of simple faults and geometries are beneficial to understand seismic sections with faults and structure (Angona, 1960). Hilterman (1970) used wood and paper to model synclines, anticlines, and vertical and low angle faults. An electric spark and a condenser microphone served as a source and receiver in this early experiment. Modeled seismic data collected in a water tank has shown success in comparing data processing and imaging between 2D and 3D datasets of ridge and fault models (French, 1974).

Several physical model prototypes of a simple vertical fault which ruptures a geologic surface were created to image a fault deformation zone using 2D marine seismic measurements. The seismic data were acquired at the University of Calgary Seismic Physical modeling Facility which is maintained by the Consortium for Research in Elastic Wave Exploration Seismology (CREWES).

Seismic resolution

The quality of seismic imaging over a fault zone is constrained by seismic resolution. Both vertical and lateral resolution is controlled by spectral bandwidth, and describes the ability to distinguish separate features (Yilmaz, 1987, p. 468). Spectral bandwidth is defined as the standard deviation about the spectral mean, or the center frequency (Barnes, 1993). Dominant wavelength varies with velocity and dominant seismic frequency, and is given by:

$$\lambda = v/f, \tag{1}$$

where λ= wavelength, v= velocity, and f = dominant frequency. Vertical seismic resolution is defined by Widess (1973) as the thickness equal to one eighth of the dominant seismic wavelength. However, one quarter of the predominant wavelength is taken as an industry standard for thin bed vertical resolution as the Widess threshold does not account for noise and wavelet broadening due to attenuation of higher frequencies with depth. Vertical resolution is important in imaging the vertical throw of a fault.

Lateral resolution threshold is determined by the Fresnel zone, an area of constructive reflection accumulation surrounding a reflection point (Lindsey, 1989). The radius of the Fresnel zone is given by the approximation:

$$r \cong (v/2)\sqrt{(t/f)} \quad (2)$$

where r= radius of the Fresnel zone, v= velocity, t=time, f= frequency. Two reflecting points that fall within the Fresnel zone are considered irresolvable, therefore lateral resolution improves as the Fresnel zone narrows. The deformation zone of shallower faults is more resolvable than deeper faults, as the Fresnel zone increases in area with depth.

Physical modeling

The physical models

The displacement and deformation zone of the Greendale Fault, which was ruptured during the 2010 Darfield earthquake, served as a general guide in creating the fault models. The Greendale fault surface rupture was mainly dextral strike-slip with 2.5 m average displacement, vertical displacement less than 0.75 m, and a 30 to 300 m wide deformation zone (Van Dissen et al., 2011). Pure strike slip faults are often difficult to detect in seismic imaging due to lack of significant vertical displacement (Fossen, 2010, p.356). Fault zones also show reduced seismic velocities which are associated with densely cracked and fractured rocks, altered rock composition, and near-surface fault gouge material (Mooney and Ginzburg, 1986).

Given these considerations, several physical model prototypes were constructed to best represent a vertical fault that ruptures the surface. Several types of materials are used to create the models and are summarized in Table 1. The velocities of the materials were measured with a Tektronix TDS 420A 200 MHz 4 Channel Digital Real-Time Oscilloscope. All of the models had 2D zero-offset seismic reflection surveys acquired as a quality check.

Table 1: Summary of physical model prototypes

	Model 1		Model 2		Model 3		Model 4		Model 5	
	Model material	Fault zone infill	Model material	Fault zone infill	Model material	Fault zone infill	Model material	Fault zone infill	Model material	Fault zone infill
	Plaster of Paris	Lard	Sandstone	Epoxy	Limestone	Wax	Limestone	Water	Limestone	Liquid Acrylic
Density (g/cm^3)	1.3	0.98	2.6	1.7	2.9	1.1	2.9	1.0	2.9	1.2
Measured Velocity (m/s)	2035	1490	2965	2680	5100	1510	5100	1480	5100	2460

.

The model and seismic acquisition measurements are scaled, where 1 mm in the physical modeling world is equivalent to 10 m in field equivalents (1:10,000). Ultrasonic modeling frequencies of 100 kHz to 1,000 kHz are scaled down by the scaling factor of 10,000 to represent real-world seismic frequencies of 10 Hz to 100 Hz. All referred measurements are scaled to represent field values and measurements.

The Plaster of Paris-Lard model (Model 1) has an average thickness of 285 m. Issues arose with this model due to air bubbles setting in the plaster as it dried, and the lifespan of the model was limited as the seismic surveys were acquired in water. The Sandstone-Epoxy model (Model 2) has an average thickness of 248 m and one side was uplifted by 30 m. The epoxy had set too quickly and only a constant width fault gap width of 30 m was created. An additional model was created with Portland cement using coarse grained sand. The model was sturdy; however scaled grain sizes of the rock would be equivalent to 5 m. These unrealistic grain sizes contribute to point scattering in a seismic reflection survey. The limestone model (Model 5) with an average thickness of 300 m, showed greatest promise as potential modeling material.

Different fault-zone infill materials were tested: water, lard, wax, epoxy, and finally acrylic plastic. A material was sought which had a higher velocity than paraffin wax and lard, which was close to the velocity of water. The epoxy used with the sandstone had a higher velocity of 2680 m/s, however, it set much too quickly, making it difficult to work with. The final fault infill material selected was a liquid acrylic (2460 m/s) which sets to a hard resin. The limestone model was fixed in place with putty, and sealed with wax to prevent leakage. The model was also uplifted on one side by approximately 10 m. At this point in the study, the limestone models with both a water-filled and acrylic-filled fault zone were considered optimal, and the results are compared in further analysis.

Physical modeling data acquisition and processing

The University of Calgary Seismic Physical Modeling Facility supports both acoustic and elastic modeling. For this study, only the acoustic modeling is considered. Dynasen Inc. CA1136-12 piezoelectric pin transducers (305mm long and 24mm diameter) acting as an acoustic source and receiver are carried in a carriage attached to a beam which moves along aluminum tracks. The transducers produce and detect vibrations with particle motion in the vertical direction (Wong et al., 2011). The modeling systems are described in further detail by Cheadle et al. (1985), Lawton et al. (1989), Gallant et al. (1991), and Wong et al. (2009a).

The physical models were immersed in a water tank for seismic acquisition modeling. Each model was placed on top of an aluminum plate, which rested on a phenolic resin block. A schematic of the Limestone model in the tank is shown in Figure 1. The models were placed in the tank with the fault length parallel to the N-S direction of the room, representing the x-axis, with the thinner end of the fault in the positive x-axis direction (Figure 2). A zero-marker was placed on all the models for coordinate reference and was located approximately 120 m East of the fault (Y=+120).

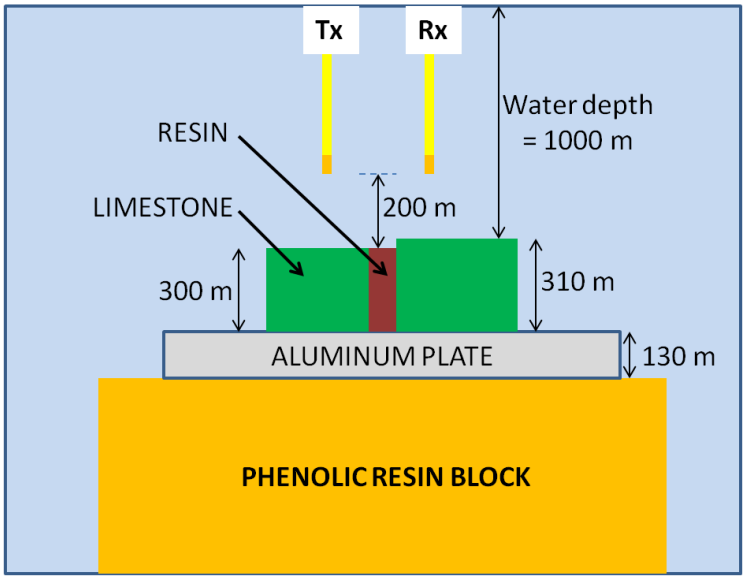

Figure 1: diagram of seismic acquisition over the final limestone model with corresponding field dimensions.

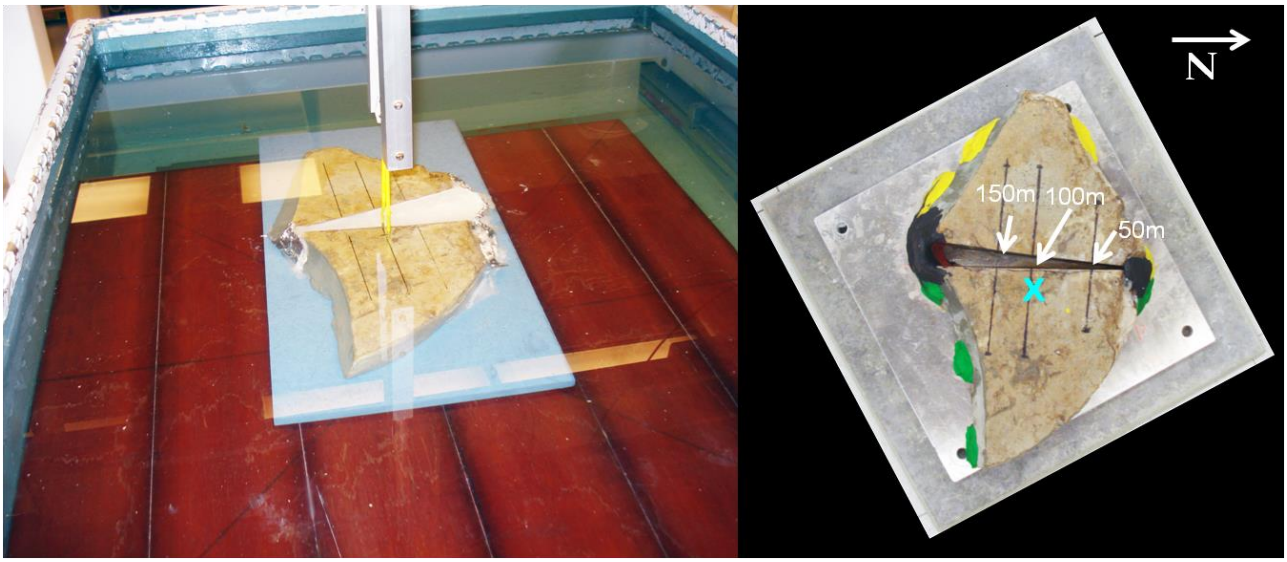

Figure 2: The Limestone-Wax model in the physical modeling water tank (left), and the limestone model (right), held in place by putty prior to fault zone infill. The blue 'x' signifies the zero marker location.

A zero-offset section, acquired by a coincident source and receiver which step along the seismic profile, was acquired for quality control of all the models to determine suitability for further investigation. Although the transducers were not exactly coincident due to the carriages, they are near-offset, with a spacing of 5 mm (50 m, scaled), and the data are processed assuming a coincident source and receiver. The zero-offset profiles ran perpendicular to the fault length along the y-axis, with the transmitter-receiver pair moving in 5 m increments with a 50 m offset in line with the fault. For the final limestone models, the total survey offset was 1600 m, and crossed three fault zone widths of 50, 100, and 150 m, respectively.

Common-source gathers were acquired for the Limestone models over the 50 m fault width. The total survey offset for the Limestone models was 1000 m. The source increment spacing was 10 m, and 101 shots were collected perpendicular across the fault length. The receiver spacing was 5 m and 201 traces were collected in each shot gather. A sample rate of 1 ms (scaled units) was used during all acquisition. For comparison with the common-source data, only the zero-offset data from the 50 m fault gap will be discussed.

The seismic data was initially viewed in Seisee for quality control, and then processed in GEDCO's VISTA seismic data processing software. Two processing flows were developed: a processing flow for the zero-offset data, and a flow for the common-source data.

Event identification

Event identification by arrival times in the processed results was done by numerical raytracing, which assumes the raypaths obey Snell's law and velocities are known (Sheriff, 1991, p. 242). Reflection events are identified by calculating the two-way travel times labeled on raw shot 101 of the Limestone-Water common source model (Figure 3a). Figure 3b illustrates the ray paths taken for each labeled event.

Down-going events (Event E and F) are surface ghosts, while the other events listed are up-going primaries. The ghost reflections identified are interesting as they do not interfere with the primary up-going reflections for this dataset, and may be useful in further imaging as an additional topic. When the water surface acts as a mirror reflecting the subsurface, 'mirror imaging' uses receiver ghosts (Grion et

al., 2007). In fact, multiples can be imaged separately from primaries to provide a better illumination of the subsurface (Wang et al., 2012).

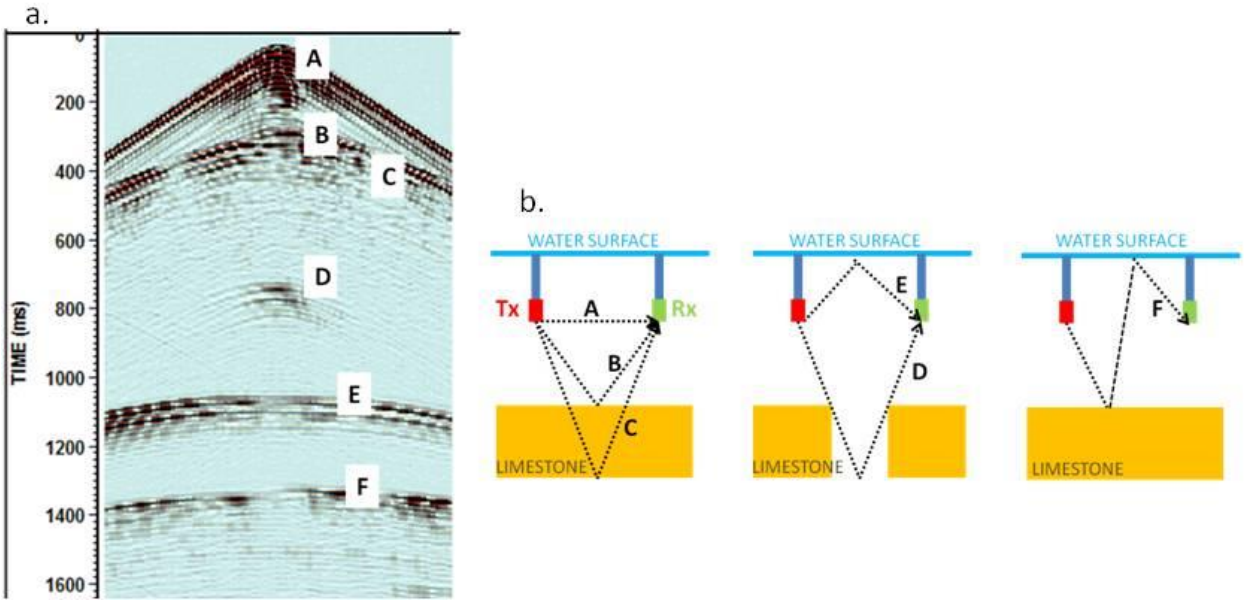

Figure 3: a) Event identification by ray tracing. A: Direct arrival (~32 ms), B: Water bottom/top of fault (~270 ms), C: Bottom of limestone (~380-400 ms), D: Bottom of water filled fault (~720 ms), E: Source ghost (~1020 ms), F: Receiver ghost/multiple of water bottom (~1275 ms). b) Illustration of the events transmitted and received by the transducers. The ray paths taken through water and the model are used to calculate expected arrival time.

Results

The final processed images of the Limestone model for a water filled and acrylic filled faults are compared in Figure 4. The surface of the 50 m fault with 10 m uplift is easily identified in all the images; however, the imaging quality of the deformation zone varies between the common-source and zero-offset data. Errors in velocity analysis of common-shot data can result in lower signal-to-noise in the stack, and mis-positioning after migration. The constant velocity used for migrating the zero-offset data is limiting if complex structure is involved.

The bottom of the limestone is better resolved in the zero-offset sections. This is most likely due to difficulty in picking this event during velocity analysis. The water bottom of the fault is most apparent again, in the zero-offset section, at approximately 720 ms. The bottom of the acrylic fault is calculated to be close to 510 ms, and again, is imaged better in the zero-offset section.

A 2D poststack time migrated seismic section of the New Zealand Greendale fault is shown in Figure 5. This seismic land data was collected by CREWES in April, 2011 and processed by Sensor Geophysical. A similar fault throw and wide fault zone is observed in both the physical modeled and field seismic sections.

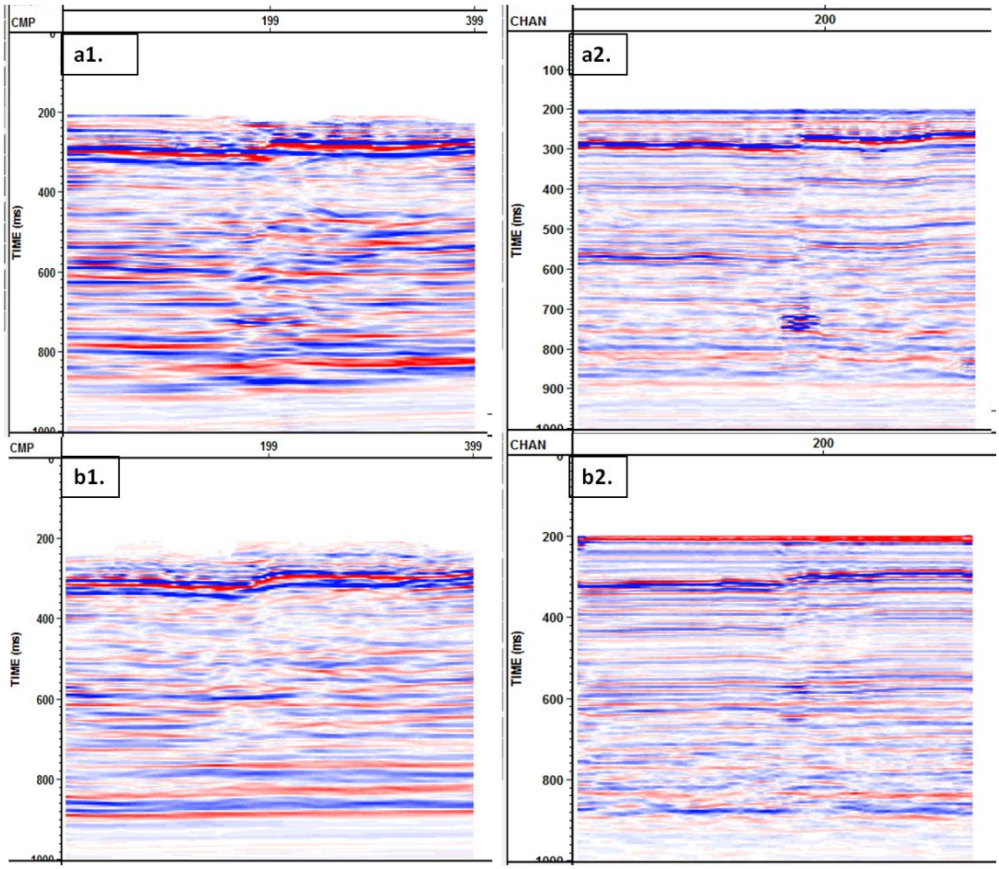

FIGURE 4: Final postmigrated images of the modeled fault zone. a1) Common-source Limestone-Water fault model. a2) Zero-offset Limestone-Water fault model. b1) Common-source Limestone-Acrylic fault model. b2) Zero-offset Limestone-Acrylic fault model.

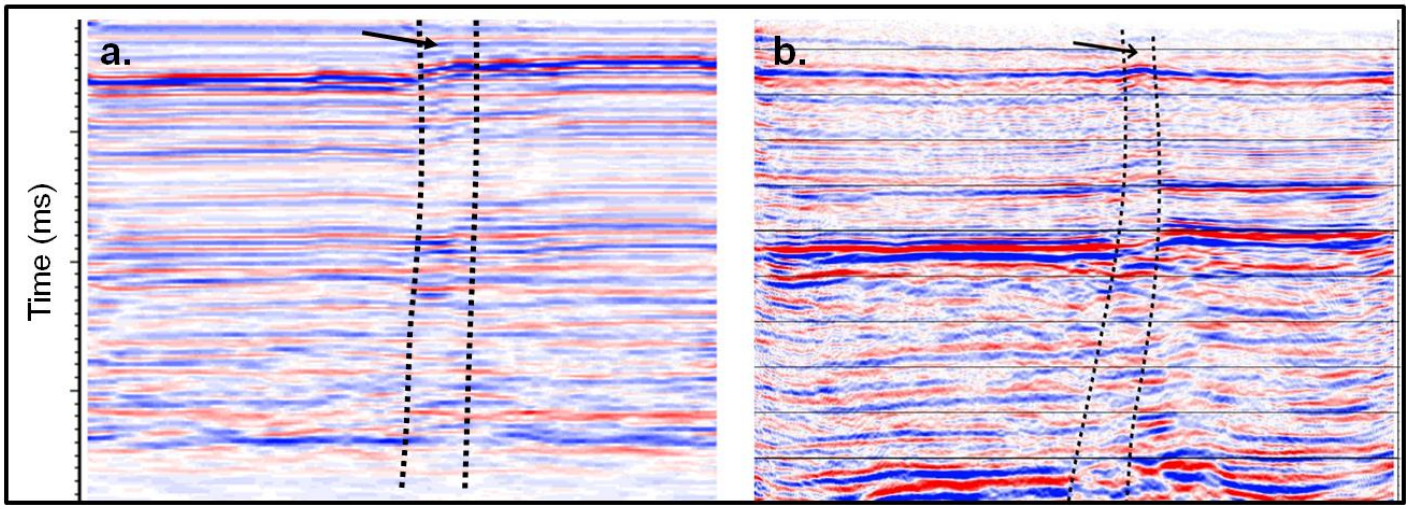

FIGURE 5: Post-stack migrated seismic sections imging a fault rupturing the surface for a) the physical model b) the Greendale fault zone, New Zealand. The deformed fault zone is outlined.

Conclusions

Physical modeling provides a method to test seismic acquisition parameters for detecting fault resolution. Consideration must be taken when designing a physical model to best represent a realistic geologic model. Selection of materials is important especially when considering attenuation, scaled geologic properties, and the ability to withstand long durations in water.
Processed model data yielded images that resolved a shallow fault with a small vertical throw and a deformed fault zone, similar to a field survey across a recent active fault in New Zealand. Resolution of seismic data is controlled not only by bandwidth, but acquisition and data processing parameters as well.

Now knowing the limitations of physical modeling, future work includes constructing a new model with a more complex fault deformation zone, and a greater depth. Numerical modeling would also be an asset to this project. As well, an interesting side topic which came to light in this project includes mirror imaging of the ghost reflections to better image the zone of interest.

Acknowledgements

We thank Rick Arthur and Eric Gallant for helping create the physical models, and Malcolm Bertram, for help with data geometry and initial processing. Thanks to GEDCO for use of VISTA seismic processing software. In addition, a sincere thank you to the CREWES sponsors for their support of this research.

References

Angona, F.A., 1960, Two-dimensional modeling and its application to seismic problems: Geophysics, **25**, 468-482, doi: 10.1190/1.1438719.

Aydin, A., 2000, Fractures, faults, and hydrocarbon entrapment, migration and flow: Marine and Petroleum Geology, 12, 797-814, doi:10.1016/S0264-8172(00)00020-9.

Barnes, C., 1993, Instantaneous spectral bandwidth and dominant frequency with applications to seismic reflection data: Geophysics, 58, 419-428, doi: 10.1190/1.1443425.

Berg, R.R., and A.H. Avery, 1995, Sealing Properties of Tertiary Growth Faults, Texas Gulf Coast: AAPG Bulletin, 79, 3, 375-379.

Cheadle, S.P., M.B. Bertram, and D.C. Lawton, 1985, Development of a physical seismic modelling system, University of Calgary: Current research part A, Geological Survey of Canada, Paper no. 85-1A, 499-504.

Das, I., and M. Zoback, 2011, Long-period, long-duration seismic events during hydraulic fracture stimulation of a shale gas reservoir: The Leading Edge, 30, 7, 778–786, doi: 10.1190/1.3609093

Fossen, H., 2010, Structural Geology: Cambridge University Press.

French, W.S., 1974, Two-Dimensional and three-dimensional migration of model-experiment reflection profiles: Geophysics, 39, 265-277, doi: 10.1190/1.1440426.

Gallant, E.V., D.C. Lawton, and M.B. Bertram, 1991, Development of a physical modelling system for 3-C x 3-D experiments. CREWES Research Report, 33, 524-528.

Grion, S., E. Russell , M. Manin, X. Miao, A. Pica, Y. Wang, P. Granger, and S. Ronen, 2007, Mirror imaging of OBS data, First Break, 25, 37-42, doi:10.3997/1365-2397.2007028.

Hennings, P., P. Allwardt, P. Pijush, C. Zahm, R. Reid, H. Alley, R. Kirschner, B. Lee, and E. Hough, 2012, Relationship between fractures, fault zones, stress, and reservoir productivity in the Suban gas field, Sumatra, Indonesia: AAPG Bulletin, 96, 4, 753-772, doi: 10.1306/08161109084.

Hilterman, F.J., 1970, Three-dimensional seismic modeling: Geophysics, 35, 1020-1037, doi: 10.1190/1.1440140.

Kaiser , A.E., H. Horstmeyer, A.G. Green, F.M. Campbell, R.M. Langridge, and A.F. McClymony, 2011, Detailed images of the shallow Alpine Fault Zone, New Zealand, determined from narrow-azimuth 3D seismic reflection data: Geophysics, 70, no. 1, B19-B31, doi: 10.1190/1.3515920.

Lawton, D.C., S.P. Cheadle, E.V. Gallant, and M.B. Bertram, 1989, Elastic physical modeling, CREWES Research Report, 19, 273-288.

Lawton, D.C., G.F. Margrave, and E.V. Gallant, 1998, Physical modeling of an anisotropic thrust, CREWES Research Report, 10, no. 15, 1-9.

Lindsey, J., 1989, The Fresnel zone and its interpretative significance: The Leading Edge, 8, 33–39, doi: 10.1190/1.1439575.

Mooney, W.D., and A. Ginzburg, 1986, Seismic measurements of the internal properties of fault zones: Pure and Applied Geophyics, 124, 141-157, doi: 10.1007/BF00875723.

Sheriff, R.E., 1991, Encyclopedic Dictionary of Exploration Geophysics: Society of Exploration Geophysicists, p. 269.

Tamagawa, T., and D.D. Pollard, 2008, Fracture permeability created by perturbed stress fields around active faults in a fractured basement reservoir: AAPG Bulletin, 92, 6, 743-764, doi:10.1306/02050807013

Van Dissen, R., D. Barrell, N. Litchfield, P. Villamor, M. Quigley, A. King, K. Furlong, J. Begg, D. Townsend, H. Mackenzie, T. Stahl, D. Noble, B. Duffy, E. Bilderback, J. Claridge, A. Klahn, R. Jongens, S. Cox, R. Langridge, W. Ries, R. Dhakal, A. Smith, S. Horblow, R. Nicol, K. Pedley, H. Henham, R. Hunter, A. Zajac, and T. Mote, 2011. Surface rupture displacement on the Greendale Fault during the Mw 7.1 Darfield (Canterbury) earthquake, New Zealand, and its impact on man-made structures. In: Ninth Pacific Conference on Earthquake Engineering: Building an Earthquake-Resilient Society, Auckland, New Zealand 14-16 Apr 2011. Accessed 9 October 2011; http://db.nzsee.org.nz/2011/186.pdf.

Vermylen, J.P., and M.D. Zoback, 2011, Hydraulic fracturing, microseismic magnitudes, and stress evolution in the Barnett shale, Texas, USA: SPE 140507. SPE Hydraulic Fracturing Technology Conference and Exhibition. 24-26 January 2011. Texas, USA.

Wang, X., C. Xia, and X. Liu, 2012, A case study: imaging OBS multiples of South China Sea, Marine Geophysical Research, 33, 1, 89-95, doi:10.1007/s11001-012-9148-2.

Widess, M.B., 1973, How thin is a thin bed?: Geophysics, 38, 1176-1180, doi: 10.1190/1.1440403.

Wong, J., R. Maier, E. Gallant, and D. Lawton, 2009a, Physical modeling of a 3D marine seismic survey, CREWES Research Report, 21, 1-10.

Wong, J., Hall, K.W., Gallant, E.V., Maier, R., Bertram, M.B., Lawton, D.C., 2009b, Seismic Physical Modelling at the University of Calgary, CSEG Recorder, 34, p. 37-43.

Wong J., F. Mahmoudian, and G. Margrave, 2011, Physical modeling III: acquiring modeled data for VVAZ/AVAZ analysis, CREWES Research Report, 23, 1-17.

Yilmaz, O., 1987, Seismic data processing: Society of Exploration Geophysicists.

Zoback, M.D., A. Kohli, I. Das, and M. McClure, 2012, The importance of slow slip on faults during hydraulic fracturing stimulation of shale gas reservoirs: SPE 155476, SPE Americas Unconventional Resources Conference, 5-7 June 2012. Pittsburgh, Pennsylvania, USA